Experimental Neurology 364 (2023) 114393

Contents lists available at ScienceDirect

Experimental Neurology

journal homepage: www.elsevier.com/locate/yexnr

Research paper

$Na_v1.7$ gain-of-function mutation I228M triggers age-dependent nociceptive insensitivity and C-LTMR dysregulation

Nivanthika K. Wimalasena [a,b,1], Daniel G. Taub [a,b,1], Jaehoon Shim [a,b], Sara Hakim [a,b], Riki Kawaguchi [c], Lubin Chen [d,e], Mahmoud El-Rifai [b], Daniel H. Geschwind [c], Sulayman D. Dib-Hajj [d,e], Stephen G. Waxman [d,e], Clifford J. Woolf [a,b,*]

[a] F.M. Kirby Neurobiology Center, Boston Children's Hospital, Boston, MA 02115, USA
[b] Department of Neurobiology, Harvard Medical School, Boston, MA 02115, USA
[c] Department of Neurology, David Geffen School of Medicine, University of California Los Angeles, Los Angeles, CA 90095, USA
[d] Department of Neurology and Center for Neuroscience and Regeneration Research, Yale University School of Medicine, New Haven, CT 06510, USA
[e] Center for Rehabilitation Research, VA Connecticut Healthcare System, West Haven, CT 06516, USA

ARTICLE INFO

Keywords:
Scn9a
Sodium channel
Nav1.7
C-LTMRs
Somatosensory insensitivity
Dorsal root ganglion

ABSTRACT

Gain-of-function mutations in *Scn9a*, which encodes the peripheral sensory neuron-enriched voltage-gated sodium channel $Na_v1.7$, cause paroxysmal extreme pain disorder (PEPD), inherited erythromelalgia (IEM), and small fiber neuropathy (SFN). Conversely, loss-of-function mutations in the gene are linked to congenital insensitivity to pain (CIP). These mutations are evidence for a link between altered sodium conductance and neuronal excitability leading to somatosensory aberrations, pain, or its loss. Our previous work in young adult mice with the $Na_v1.7$ gain-of-function mutation, I228M, showed the expected DRG neuron hyperexcitability, but unexpectedly the mice had normal mechanical and thermal behavioral sensitivity. We now show that with aging both male and female mice with this mutation unexpectedly develop a profound insensitivity to noxious heat and cold, as well skin lesions that span the body. Electrophysiology demonstrates that, in contrast to young mice, aged I228M mouse DRGs have a profound loss of sodium conductance and changes in activation and slow inactivation dynamics, representing a loss-of-function. Through RNA sequencing we explored how these age-related changes may produce the phenotypic changes and found a striking and specific decrease in C-low threshold mechanoreceptor- (cLTMR) associated gene expression, suggesting a potential contribution of this DRG neuron subtype to $Na_v1.7$ dysfunction phenotypes. A GOF mutation in a voltage-gated channel can therefore produce over a prolonged time, highly complex and unexpected alterations in the nervous system beyond excitability changes.

1. Introduction

Dorsal root ganglion (DRG) neurons innervating the skin, muscle, and viscera relay information about mechanical, thermal, and chemical stimuli to the central nervous system. The electrophysiological properties of high threshold nociceptor DRG neurons are dependent on three major voltage-gated sodium channel subtypes: $Na_v1.7$, $Na_v1.8$, and $Na_v1.9$. These channels are distributed across several different subtypes of DRGs and contribute to electrogenesis, with $Na_v1.7$ and $Na_v1.9$ contributing to the action potential threshold and $Na_v1.8$ the action potential upstroke (Rush et al., 2007). Gain-of-function (GOF), single nucleotide mutations in $Na_v1.7$ are specifically implicated in a range of painful conditions including: inherited erythromelalgia (IEM), paroxysmal extreme pain disorder (PEPD) (Dib-Hajj et al., 2013; Drenth and Waxman, 2007), and small fiber neuropathy (SFN) (Faber et al., 2012; Hoeijmakers et al., 2012; Huang et al., 2014), while recessive loss-of-function (LOF) mutations primarily result in congenital insensitivity to pain (CIP) (Cox et al., 2006; Sun et al., 2020). Canonically, pain in these conditions is directly associated with heterozygous GOF mutations with an increase in sodium conductance and neuronal hyperexcitability, whereas a lack of pain is associated with homozygous LOF, largely due to nonsense mutations, that cause DRG neuron hypoexcitability.

* Corresponding author at: F.M. Kirby Neurobiology Center, Boston Children's Hospital, Boston, MA 02115, USA.
E-mail address: clifford.woolf@childrens.harvard.edu (C.J. Woolf).
[1] These authors contributed equally to this work.

https://doi.org/10.1016/j.expneurol.2023.114393
Received 23 January 2023; Received in revised form 9 March 2023; Accepted 27 March 2023
Available online 30 March 2023

Therefore, these conditions are considered as evidence that aberrant increases or decreases in excitability in specific subsets of DRG neurons is sufficient to drive either pain or its absence, a state of persistent analgesia, respectively.

However, the relationship between sodium channel activity and pain sensitivity may be more complex than originally considered. Phenotypic presentation and age of onset can vary in patients with the same $Na_v1.7$ GOF mutation and these mutations also exist in healthy individuals with no pain disturbance (Estacion et al., 2011; Han et al., 2009). Additionally, several $Na_v1.7$ GOF mutations linked with neuronal hyperexcitability and pain, also cause loss of sensory innervation in the epidermis (Hoeijmakers et al., 2015), which is paradoxically linked to the CIP caused by biallelic LOF mutations in $Na_v1.7$ (Marchi et al., 2018). It remains unclear though how peripheral neuropathy can result from both GOF and LOF mutations in $Na_v1.7$. Finally, much of the preclinical work on these mutations has been done by an overexpression of the mutant channels in mouse DRG neurons or in immortalized cell lines, which has caveats, because it is likely that a complex genetic and environmental landscape may be a factor in the development of the disease phenotype in these patients.

We recently generated two-independent mouse lines where the endogenous murine $Na_v1.7$ channel was edited at a single base using either homologous recombination or CRISPR/Cas9. This approach avoids potential overexpression artifacts (Chen et al., 2021). We focused on the I228M GOF $Na_v1.7$ mutation, which produces both pain and neuropathy in patients (Estacion et al., 2011; Lee et al., 2020; Persson et al., 2013). While the expected DRG neuron hyperexcitability in young mice was detected in our first study, unexpectedly, no evidence of a pain phenotype was observed at the same age (8–12 weeks), suggesting that even in the presence of hyperexcitable DRG neurons, other factors are required to cause those pain-related behaviors in mice that can be detected using current preclinical methodologies (Chen et al., 2021).

Since the clinical presentation of symptoms in I228M patients can appear late in life (Estacion et al., 2011), we now assessed the sensory and behavioral phenotypes of I228M GOF $Na_v1.7$ mutant mice at old ages, and unexpectedly found a profound insensitivity to thermal stimuli, the development of skin lesions, and changes in neuronal activity and gene expression, that together suggest that aging in mice with the GOF mutation eventually produces a phenotype that is more consistent with a LOF of $Na_v1.7$. We further find a specific disruption of C-low threshold mechanoreceptors (cLTMRs), which we hypothesize contributes to the behavioral changes. Generation of a single GOF mutation in a voltage-gated sodium channel can result, therefore, in highly complex age-dependent changes which go beyond a simple increase in sensory neuron excitability and may reflect more the compensatory changes in response to the altered excitability, and these may well account for the complexity of sodium channel mutation clinical phenotypes.

2. Materials and methods

All mouse work at Boston Children Hospital was carried out in accordance with IACUC protocols 17–06-3494R and 20–05-4208R. Mice of both sexes were used in all studies.

Behavioral Methods:

2.1. Noxious heat sensitivity assay

A hot plate was set at 50 °C. Animals were placed on the plate and the latency to hind paw licking or jumping recorded. After 75 s the mice were removed from the plate if there was no response. Mice were tested only once to ensure they did not adapt to the assay and to avoid tissue damage.

2.2. Noxious COLD SENSITIVITY ASSAY

Animals were habituated for 1 h to plastic chambers with a metal grate bottom on two separate days. 30 μL of the evaporative coolant acetone was placed on the hindpaw and the amount of time spent flinching, shaking, or biting the paw recorded within a 30 s time window.

2.3. Mechanical sensitivity assay (Von Frey)

Animals were habituated for 1 h to plastic chambers with a metal grate bottom on two separate days. Von Frey was performed by the Up-Down method.

2.4. Noxious mechanical sensitivity assay (pinprick)

Animals were habituated as above for Von Frey. A pin was pricked on the hindpaw 5 times and nocifensive behavior recorded.

2.5. Scratching behavior recordings

The animals were enclosed in a device termed the iBob (Wimalasena et al., 2021) containing a lower habituation chamber and upper recording chamber. Each chamber contained an opaque six-chambered plastic enclosure atop a glass floor. The box was dark and illuminated with only infrared light. Animals were habituated for one hour then moved to the recording chamber where they were recorded for 1 h with a camera from below. Up to six mice were imaged from below simultaneously and scoring of scratching behavior was done manually on the latter 30 min of each video.

2.6. Chloroquine

The nape of the neck was shaved and mice were allowed to acclimate to the chamber on two consecutive days for 30 min each. Baseline recordings in the iBob (mentioned above) were recorded for 30 min. The next day, mice were injected with 8 mM Chloroquine subcutaneously and recorded again for 30 min. The numbers of scratching bouts in 30 min were determined in a blinded fashion for each animal.

3. Voltage and current clamp recording

Whole-cell patch-clamp recordings in mouse DRG neurons in PDL/Laminin-coated 35 mm dishes (Falcon) were performed at room temperature. Only small-diameter neurons (<25 μm) were recorded. The extracellular solution contained: 30 mM NaCl, 90 mM Choline-Cl, 20 mM TEA—Cl, 3 mM KCl, 1 mM $CaCl_2$, 1 mM $MgCl_2$, 0.1 mM CdCl 10 mM HEPES, 10 mM Dextrose; pH was adjusted to 7.4 with NaOH, and osmolality was adjusted to 300–310 mOsm with sucrose. A recording electrode (1.8–3.0 MΩ) was filled with pipette solution (140 mM CsF, 10 mM NaCl, 1.1 mM EGTA, 10 mM HEPES, 20 mM Dextrose); pH was adjusted to 7.3 with CsOH, and osmolality was adjusted to 280–290 mOsm with sucrose. Pipette and cell capacitance were minimized using Multiclamp 700B amplifier (Molecular Devices). Series resistance was compensated and predicted for 80%–90%. The recorded currents were digitized at 100 kHz and low pass filtered at 10 kHz using pClamp10.5 and Digidata 1440A (Molecular Devices). The Na^+ current recording was initiated 5 min after the whole-cell configuration was held at -70 mV. Series resistance (R_s) and capacitance (C_m) values were taken directly from readings of the amplifier after electronic subtraction of the capacitive transients.

Capacitive and leakage currents were digitally subtracted using a *P/N* leak subtraction protocol from a holding potential of −120 mV. ValveBank II (Automate Scientific) was used to change the flow bath solution, and 100 nM TTX (Tocris) was used to isolate TTX-S current using digital subtraction in Clampfit 10.5 (Molecular Devices). Data were graphed and fitted using Prism 8 (GraphPad).

To generate activation curves, cells were held at −120 mV. Voltage-gated Na currents were evoked with a series of 100 ms command

potentials from −80 to 40 mV. Peak inward currents were converted to conductance using the equation, $G_{Na} = I_{Na}/(V_m\text{-}E_{Na})$, for which G_{Na} is the conductance, I_{Na} is the peak inward sodium current, $V_m\text{-}E_{Na}$ is the driving force where V_m is the membrane potential step, and E_{Na} is the reversal potential for sodium. Conductance was normalized by maximum conductance value and fitted with a Boltzmann eq. $G = G_{min} + (G_{max}\text{-}G_{min})/(1 + \exp.[(V_{1/2}\text{-}V_m)\text{-}V_m/k]$, where $V_{1/2}$ is the half-maximal activation voltage, and k is the slope factor (a positive number for activation, a negative one for inactivation). To generate steady-state fast-inactivation curves, cells were held at −120 mV and stepped from −140 to 10 mV for 500 ms, followed by a 20 ms step to -10 mV. Peak inward currents from the steady-state fast-inactivation were normalized by the maximum current amplitude and fitted with a Boltzmann eq. $I = I_{min} + (I_{max}\text{-}I_{min})/(1 + \exp.[(V_m\text{-}V_{1/2})/k]$, where $V_{1/2}$ is the half-maximal inactivation voltage. Small DRGs(<25um) with more negative than −40 mM RMP were analyzed. RMP was measured right after the rupture. Threshold was determined with 5pA increment of current injection for 200 mM to find the current that generates the first action potential. Action potentials elicited by a series of depolarizing current steps for 500 ms were counted for the current step experiment.

3.1. Bulk RNA sequencing

All DRG neurons (cervical, thoracic, lumbar) were dissected from WT ($n = 2$), HetNa$_v$1.7^{I228M} ($n = 4$), and HomNa$_v$1.7^{I228M} ($n = 6$) mice at 20 weeks of age according to standard protocols. Samples from each mouse were treated individually. Upon dissection, DRGs were frozen on dry ice and subsequently stored at −80 °C prior to shipment to UCLA for processing. RNA samples were sequenced by the UNGC. Samples were pooled and barcoded. Library was prepared using TruSeq Stranded RNA (100 ng) + RiboZero Gold. Preparation included 75 bp paired end reads and sequencing run was carried out over 2 lanes. Reads were aligned to the latest mouse mm10 reference genome using the STAR spliced read aligner. Total counts of read fragments aligned to known gene regions within the mouse mm10 refSeq reference annotation were used as the basis for quantification of gene expression. Fragment counts were derived using HTS-seq program using mm10 Ensembl transcripts as model. Various QC analyses were conducted to assess the quality of the data and to identify potential outliers. Differentially expressed genes were identified using three bioconductor packages, edgeR, limma+voom and limma which are then considered and ranked based on adjusted *p*-values (FDR) of <0.1. Differentially expressed gene lists from all three analyses were similar. Fold change and p-values used in the manuscript come from the limma analysis (Ritchie et al., 2015). Gene set enrichment analysis (GSEA) was performed on the entire data set as well as the top 100 differentially expressed genes. GO Term Analysis plot was generated by g:Profiler version e107_eg54_p17_bf42210 to illustrate these findings (Raudvere et al., 2019). The clustering of differentially expressed genes was done by taking the top 100 genes by limma analysis and using a variance stabilization transform and then applying a Euclidean distance function to generate the heatmap data.

3.2. RNAScope of DRGs

Thoracic DRGs were dissected from WT and HomNa$_v$1.7^{I228M} mice at 2 weeks, 8 weeks, and 20 weeks of age ($n = 3$ WT at each 2 weeks and 20 weeks, n = 3 HomNa$_v$1.7^{I228M} at each 2 weeks, 8 weeks, and 20 weeks). DRGs were immediately fresh frozen in Tissue-Tek OCT compound (4583, Sakura Fintech, USA) (appx. 6 DRGs/block) and stored at −80 °C prior to sectioning. Blocks containing DRGs were cryosectioned at a thickness of 20 μm and mounted on SuperFrost Plus Microscope slides (12–550-15, Fischer Scientific). Each slide contained DRGs from both genotypes to control for slide-to-slide variation. RNAScope probes used were against Tubb3 (Tubulin, beta 3 class III) (423391-C2, Advanced Cell Diagnostics), Th (Tyrosine Hydroxylase) (317,621, Advanced Cell Diagnostics), and Slc17a8 (Vesicular Glutamate Transporter 3) (431261-C3, Advanced Cell Diagnostics) and was done according to the standard protocol from the RNAScope Fluorescent Multiplex Kit (Advanced Cell Diagnostics).

Briefly, fresh frozen sections were fixed for 15 min with 4% PFA, and then dehydrated using EtOH. Sections were then treated with protease III for 30 min at room temperature (RT). Probes were warmed to 40 °C for 10 min and then cooled to RT. The probes were mixed at a 50:1:1 ratio (C1:C2:C3) and then added to each section. The slides were then incubated at 40 °C for 2 h to hybridize the probes. Afterward, the slides were incubated with an amplification regent for each channel in sequence (AMP-1 FL for 30 min at 40 °C, followed by AMP-2 FL for 15 min at 40 °C, followed by AMP-3 FL for 30 min at 40 °C, followed by AMP-4 FL for 15 min at 40 °C). Slides were washed between each step. Finally, they were incubated with DAPI for 1 min at RT, and then coverslips were mounted and sealed.

Imaging of slides was done on an Ultraview Spinning Disk Confocal Microscope or Leica SP8 at 40× or 60× magnification. Images of the entire DRG in each section were captured by tiling these images. Tiled images were imported into ImageJ and neurons positive for each probe were manually counted.

3.3. Intraepidermal nerve fiber density analysis

Nerve fiber density of the hindpaw skin was performed by taking a 3 mm biopsy and fixing overnight in Zamboni fixative at 4 °C. Biopsies were then placed in 30% sucrose for two days before embedding in OCT, freezing, and storing at −80 °C. Cryosections, 12 μm thin, were then mounted on slides and dried. For immunostaining, slides were brought to room temperature, rinsed for 10 min with 1 X PBS, rinsed in 1 X PBS with 0.3% Triton-X100 for 10 min three times, and then blocked for two hours with buffer containing 1 X PBS with 0.3% Triton-X100 and 10% normal donkey serum. Slides were incubated with rabbit anti-PGP9.5 (1:100 Abcam #ab108986) overnight. Slides were then washed with 1 X PBS three times for 10 min each before incubating with Donkey anti-Rabbit Cy3 (1:500 Jackson Immunoresearch #711–165-152) for two hours. Slides were then washed with 1 X PBS three times for 10 min each before coverslipping and mounting with DAPI mounting media. Slides were imaged with a Leica SP8 tiling confocal microscope and nerve fiber density was calculated by counting the number of nerve fibers that reach the epidermis normalized to the length of the section.

3.4. qPCR of DRGs

All DRGs were dissected from WT and HomNa$_v$1.7^{I228M} mice at 2 and 20 weeks of age. DRGs were placed in TRIzol (15,596,026, Invitrogen) and frozen at −20 °C until the time of the experiment. Samples were thawed and DRGs were homogenized with a pellet homogenizer (Z359971, Sigma Aldrich) for several minutes. Samples were then manually triturated several times with a 5 mL syringe and 25G needle to further break up the DRGs. RNA was extracted using a standard protocol (https://assets.thermofisher.com/TFS-Assets/LSG/manuals/trizol_reagent.pdf) and cDNA was generated using the SuperScript VILO cDNA Synthesis Kit (11,754,250, Invitrogen). Samples were assessed by qPCR in duplicate using both *Hprt* and *Gapdh* as housekeeping genes. Because results were similar, and due to higher expression of *Hprt* in the samples, data using *Hprt* are shown in the manuscript. The fold change of expression of HomNa$_v$1.7^{I228M} samples were compared to WT using the $\Delta\Delta C_t$ method. In experiments with more than one WT control, HomNa$_v$1.7^{I228M} samples were compared to the average of the WT samples. Primers sequences used are provided below.

Th	F	5'-GTCACGTCCCCAAGGTTCAT-3'
	R	5'-ACCTCGAAGCGCACAAAGTA-3'
Scn9a	F	5'-TGGATTCCCTTCGTTCACAGA-3'
	R	5'-GTCGCAGATACATCCTCTTGTTT-3'
Slc17a8	F	5'-AGAATGCCGTGGGAGACTC-3'

(*continued on next page*)

(*continued*)

	R	5'-CAGTCACAGATGTACCGCTTG-3'
Gapdh	F	5'-CTGGGCTACACTGAGCACC-3'
	R	5'-AAGTGGTCGTTGAGGGCAATG-3'
Hprt	F	5'-CAGTCCCAGCGTCGTGATTA-3'
	R	5'-TGGCCTCCCATCTCCTTCAT-3'

3.5. Western blotting of DRGs

DRGs from WT, HetNa$_v$1.7^{I228M}, and HomNa$_v$1.7^{I228M} mice >20 weeks of age were taken and rapidly frozen on dry ice. Protein was isolated by lysing the DRGs in RIPA Buffer (ThermoScientific) in the presence of protease inhibitors using the Precellys 24 system (Bertin Technologies). Protein was then quantified and normalized using Pierce BCA Protein Assay Kit (ThermoScientific). Equal amounts of protein were loaded onto a 10–20% Tris Glycine Gel (Invitrogen) in 4× SDS protein loading buffer (Licor) and run at 225 V for 1.5 h. Protein was transferred to low autofluorescence PVDF membrane, blocked with Intercept TBS Blocking Buffer (Licor) for 1 h, and incubated overnight in blocking buffer at 4 °C with anti-Nav1.7 antibody (1:500 Alomone Labs acs-008) and anti-beta tubulin (1:1000 Sigma Aldrich T8660). The membrane was rinsed with TBS and probed with secondary antibodies in blocking buffer (goat anti-rabbit CW800 #925–32,211 and goat anti-mouse 680RD #926–68,070–1:10,000) for 1 h. The membrane was rinsed and imaged with the LiCor Odyssey Dlx. Protein bands were quantified by measuring the density of Nav1.7 and normalizing it to beta-tubulin (Fiji/ImageJ).

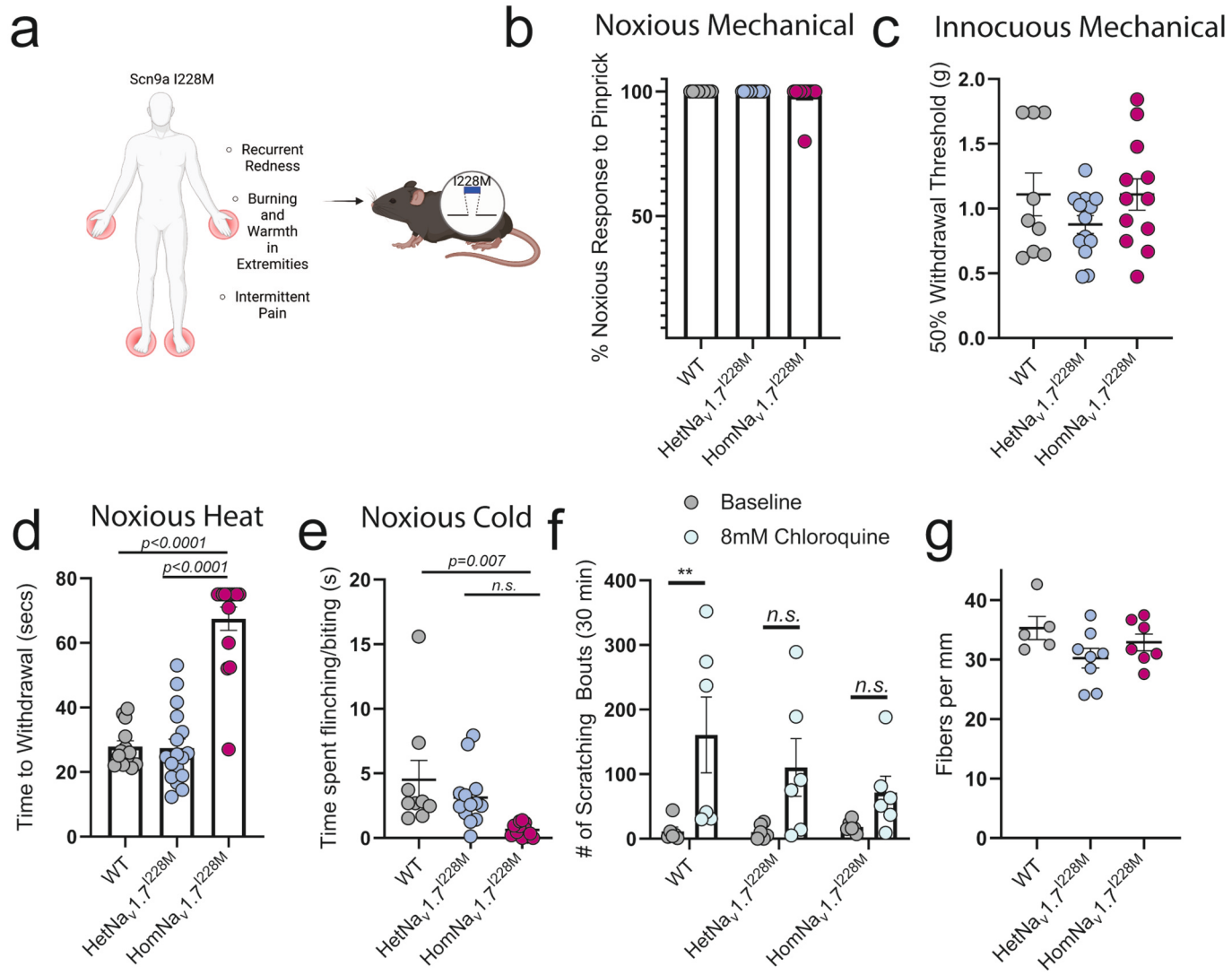

Fig. 1. HomNa$_v$1.7^{I228M} mice display resistance to noxious temperatures and pruritogenic stimuli.
A) Schematic diagram of the approach to generating I228M mutant mice by CRISPR/Cas9 and comparison with some of the common symptoms of I228M-related disease in patients. B) Sensitivity to noxious mechanical stimuli via pinprick. (n = 9, 13, and 12 for WT, HetNa$_v$1.7^{I228M}, and HomNa$_v$1.7^{I228M}, respectively. One-way ANOVA n.s.) C) Sensitivity to innocuous mechanical stimuli via Von Frey filaments (n = 9, 13, and 12 for WT, HetNa$_v$1.7^{I228M}, and HomNa$_v$1.7^{I228M}, respectively. One-way ANOVA n.s.). D) Thermal sensitivity assayed with a 50 °C hot plate for 75 s. Latency to hind paw licking in response to the noxious temperature is significantly higher in HomNa$_v$1.7^{I228M} animals compared to WT and HetNa$_v$1.7^{I228M} littermate controls (n = 13, 17, and 15 for WT, HetNa$_v$1.7^{I228M}, and HomNa$_v$1.7^{I228M}, respectively. One-way ANOVA with Tukey's multiple comparisons ***-$p < 0.0001$. E) Sensitivity to noxious cold in the acetone assay (n = 9, 13, and 12 for WT, HetNa$_v$1.7^{I228M}, and HomNa$_v$1.7^{I228M}, respectively. One-way ANOVA Tukey's posthoc ** - $p = 0.007$). F) Sensitivity to the pruritogen chloroquine, as assayed by number of scratching bouts in 30 min post injection. (n = 6 animals per group, Two Way ANOVA with Sidak's multiple comparisons test ** - $p = 0.01$). G) Intraepidermal nerve fiber density measured by examining PGP9.5 positive fibers in the plantar surface of the hindpaw. (n = 5, 8, and 7 for WT, HetNa$_v$1.7^{I228M}, and HomNa$_v$1.7^{I228M}, respectively. One-way ANOVA n.s.).

3.6. Comparison to Minett et al. 2015 dataset

This dataset is publicly available at GEO Accession GSE61373. We used GEO2R to compare WT samples (DRG_WT_1.7_1, DRG_WT_1.7_2, DRG_WT_1.7_2) with $Na_v1.7^{cKO}$ samples (DRG_KO_1.7_1, DRG_KO_1.7_2, DRG_KO_1.7_3) and used the standard settings, with a Benjamini & Hochberg (False discovery rate) correction to the *p*-values and an FDR adjusted p-value cutoff of <0.05. We then compared the list of significantly differentially expressed genes to our dataset. The same was done with $Na_v1.8^{KO}$ and $Na_v1.9^{KO}$ samples.

4. Results

4.1. $HomNa_v1.7^{I228M}$ mice develop an insensitivity to noxious temperature and pruritogenic stimuli with age

As somatosensory/pain conditions in patients with *Scn9a* mutations, including patients with I228M, often present late in life, we decided to evaluate I228M mutant mice aged over 18 weeks of age, corresponding to middle-age (Fig. 1a). We performed several assays for peripheral sensitivity, including von Frey and pinprick for low and high intensity mechanical sensitivity, hot plate for noxious heat, and acetone for noxious cold. While the mechanical sensitivity to noxious and non-noxious stimuli was unaffected (Fig. 1b and c), consistent with our earlier observations in younger (<12 week old) animals (Chen et al., 2021), aged (>18 weeks) $HomNa_v1.7^{I228M}$ animals surprisingly were insensitive to noxious heat and cold. $HomNa_v1.7^{I228M}$ animals had an increased latency to paw withdrawal on a 50 °C hot plate, and many (66%) did not respond for the entire duration of the 75 s testing period (Fig. 1d WT: 28.92 s, Het $Na_v1.7^{I228M}$: 27.45 s, and $HomNa_v1.7^{I228M}$: 67.49 s One-Way ANOVA, Tukey's post-hoc between WT and Het vs. Homo $p < 0.0001$). Likewise, $HomNa_v1.7^{I228M}$ animals exposed to the noxious evaporative coolant, acetone, were largely unresponsive to the stimulus (Fig. 1e WT: 4.512 s, Het $Na_v1.7^{I228M}$: 3.13 s, and $HomNa_v1.7^{I228M}$: 0.62 s One-Way ANOVA, Tukey's post-hoc between WT vs. Homo $p = 0.007$). This was in sharp contrast to the normal sensitivity to noxious thermal stimuli observed at young (8–12 week) ages in the same mouse model (Chen et al., 2021), and now shows that $HomNa_v1.7^{I228M}$ mice display an age-dependent thermal insensitivity. As these phenotypic behavioral changes were more like that arising from $Na_v1.7$ LOF rather than GOF mutations, and resistance to chloroquine (CQ) induced itch is a known phenotype in $Na_v1.7$ LOF mice (Kuhn et al., 2020; Shields et al., 2018), we assessed if itch in these mice was altered. Injection of chloroquine on the nape of the neck produced a robust increase in scratching behaviors in WT animals. In contrast, $HomNa_v1.7^{I228M}$ mice were largely resistant to the effects of chloroquine with $HetNa_v1.7^{I228M}$ animals displaying an intermediate phenotype (Fig. 1f scratching bouts in 30 mins - WT: 11.50 vs. 160.8, $p = 0.01$; $HetNa_v1.7^{I228M}$: 10.50 vs. 110.5; $HomNa_v1.7^{I228M}$: 18.50 vs. 71.50 Two-Way ANOVA, Sidak's post-hoc tests).

As $Na_v1.7$ dysfunction in small fiber neuropathy is associated with a loss of small diameter fibers innervating the skin, and the potential that such fiber loss could explain these behavioral phenotypes described above, we performed an intraepidermal nerve fiber density analysis (Hoeijmakers et al., 2015). However, although fiber density was slightly lower in both Het and $HomNa_v1.7^{I228M}$, it was not significantly different (Fig. 1g WT: 35.31, Het $Na_v1.7^{I228M}$: 30.24, and $HomNa_v1.7^{I228M}$ 32.89 One-Way ANOVA Tukey's post-hoc n.s.). $HomNa_v1.7^{I228M}$ mice display, therefore, an unexpected and progressive loss of noxious thermal and pruritogenic sensitivity after adolescence which appears not to be due to peripheral terminal axon loss/withdrawal.

4.2. $HomNa_v1.7^{I228M}$ mice develop skin lesions with age

In addition to thermal and pruritogenic insensitivity, we found that mice >18 weeks of age begin to display skin lesions on the facial and dorsal skin (Fig. 2). Lesions also present in patients with IEM, but these are largely thought to be caused by submerging the affected body parts in cold water for relief, or in rare cases, self-mutilation (Drenth and Waxman, 2007; Arthur et al., 2019; Meijer et al., 2014). The lesions were present in both male and female mice and appeared self-inflicted, given the same phenotype was observed in singly housed animals. Co-housed WT and heterozygous ($HetNa_v1.7^{I228M}$) littermates did not display these lesions and were normal in appearance, whereas nearly all $HomNa_v1.7^{I228M}$ mice developed visible skin lesions between 15 and 30 weeks of age, typically increasing in severity over time. The localization of lesions varied from animal to animal but appeared across regions accessible to the hind paw, most commonly the face around the eyes, near the ears, and at the nape of the neck. Conversely, we did not observe lesions on the lower third of the back, where wounds secondary to fighting between animals are often found. Lesions were characterized by missing hair, broken skin, and scab formation (Fig. 2). This parallels with I228M patients with idiopathic SFN who uniquely present with proximal (facial/scalp) symptoms, which is in contrast to the canonical "stocking-glove" phenotype commonly observed in SFN (Estacion et al., 2011). As lesions were confined to the skin, we considered that these lesions could be due to either increased frequency or force of grooming/scratching behaviors. Indeed, although variable and changing with time, the number of scratching bouts in $HomNa_v1.7^{I228M}$ mice was generally higher than $HetNa_v1.7^{I228M}$ and WTs (Supplementary Fig. 1 a and b). Notably, however, even those WT or $HetNa_v1.7^{I228M}$ mice that did scratch at similar levels to $HomNa_v1.7^{I228M}$ did not display lesions, suggesting that the $HomNa_v1.7^{I228M}$ mice may scratch more intensely because of a reduced sensitivity to scratching so that it is repeated more, for longer, and with greater force (Supplementary Fig. 1 c-j). If the mouse has no means of detecting when scratching begins to damage the skin, it will likely continue beyond that point. In conjunction with the resistance to chloroquine induced scratching, this suggests a loss of pruritogenic responsiveness, similar to that observed in $Na_v1.7$ loss of function models.

4.3. $HomNa_v1.7^{I228M}$ DRGs show age-related changes in sodium current and activation/ inactivation dynamics

To understand if age changes the electrophysiological properties of $HomNa_v1.7^{I228M}$ sensory neurons, we performed whole cell voltage-clamp recordings on small-diameter DRG neurons from >20 week old $Na_v1.7^{I228M}$ mutants. We found that both the total and TTX-sensitive (TTX-S) sodium current were significantly reduced in $HomNa_v1.7^{I228M}$ neurons compared to WT, with a more pronounced effect at more hyperpolarized voltages (Fig. 3a, b, c). Given the characterization of the I228M mutant as a GOF, and evidence showing early hyperexcitability in mutant DRG neurons (Chen et al., 2021), this finding was unexpected. However, it aligns with the loss of thermal and pruritogenic sensitivity we observe behaviorally. As this decrease represented the total sodium current, it could be caused either by a decrease in $Na_v1.7$ sodium conductance or a decrease in the number of $Na_v1.7$ channels per cell. While we observed a 2-fold decrease in mRNA expression of *Scn9a* in $HomNa_v1.7^{I228M}$ DRG neurons compared to those in WT DRGs at 20 weeks of age, by both bulk RNA sequencing and qPCR (shown in Fig. 4 and Supplementary Fig. 2a, respectively), we did not observe changes in $Na_v1.7$ protein in the soma of DRGs of aged mice by Western blotting, suggesting that the change in Na^+ current may not be explained by a decrease in channel number, at least in the cell body (Supplementary Fig. 2b). It is possible that compensatory changes occur at the transcript or protein translation level, with the early enhanced electrical activity of the neurons leading to a downregulation of mRNA expression (Klein et al., 2003). Alternatively, altered channel expression or density within the peripheral or central axon terminals may be driving the phenotype. The RNA sequencing showed no truncated transcripts or other evidence that a nonsense mutation had arisen causing a LOF in the channel, making it unlikely that the decrease in sodium conductance was due to

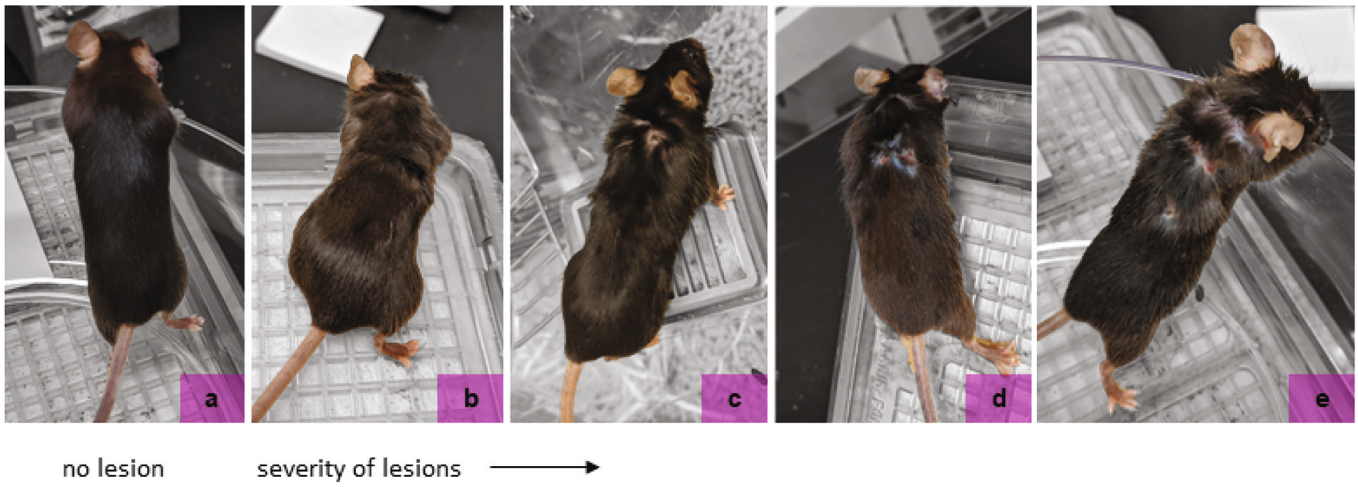

Fig. 2. HomNa$_v$1.7^{I228M} mice begin to display skin lesions >20 weeks of age.
A) Representative image of co-housed HetNa$_v$1.7^{I228M} littermate animal at 20 weeks, showing no lesions or disturbed hair. B-E) Representative images of HomNa$_v$1.7^{I228M} animals with lesions of varying severity, increasing from left to right. Lesions generally increase in severity with age for individual animals, but timing of onset and severity varies from animal to animal. Lesions appeared in both male and female HomNa$_v$1.7^{I228M} animals, as well as in animals singly housed, suggesting self-inflicted wounds, perhaps due to increased scratching or intensity or lack of its detection (Supplementary Fig. 1). No lesions were observed in WT or HetNa$_v$1.7^{I228M} littermate animals.

such a change (data not shown).

To gain additional insight into Na$_v$1.7 functional disturbances we evaluated its voltage- dependence of activation and inactivation (Table 1) and observed a slight, but significant, shift in the activation curve, with a V1/2 of −40 mV and − 35.8 mV for WT and HetNa$_v$1.7^{I228M} neurons respectively, and − 23.7 mV for HomNa$_v$1.7^{I228M} neurons (Fig. 3d, e). This was also true for the TTX-S current with a V1/2 of −39.8 mV and − 36.2 mV for WT and HetNa$_v$1.7^{I228M} neurons respectively, and − 24.8 mV for HomNa$_v$1.7^{I228M} neurons. Further, we observed a larger depolarizing shift in the voltage-dependence of inactivation in HomNa$_v$1.7^{I228M} neurons relative to WT with a $V_{1/2}$ of −82.1 mV and − 83.2 mV for WT and HetNa$_v$1.7^{I228M} neurons respectively, and − 41.7 mV for HomNa$_v$1.7^{I228M} neurons (Fig. 3f, g). A similar change was observed when looking only at the TTX-S current ($V_{1/2}$ = −87.1 mV (WT), −87.5 mV (HetNa$_v$1.7^{I228M}), −56.7 mV (HomNa$_v$1.7^{I228M})) (Fig. 3f). Although the measured TTX-S current is small in this case, this suggests a delayed activation and inactivation of Na$_v$1.7 in homozygous I228M mice, similar with other reports (Faber et al., 2012; Estacion et al., 2011), although, as the measured TTX-S current is small, these shifts in activation/inactivation may be due to minor contamination of TTX-R current due to the moderate concentration of TTX we utilized in this assay (Shields et al., 2018).

In young I228M mouse DRGs, as well as mouse DRGs transfected with the I228M channel and other putative GOF Na$_v$1.7 mutations, the number of action potentials firing was increased following a given injection of current (Faber et al., 2012; Estacion et al., 2011; Chen et al., 2021; Yang et al., 2016). However, although there is a trend toward decreased firing in aged HomNa$_v$1.7^{I228M} DRGs, we detected no significant changes in the number of action potentials evoked (Supplementary Fig. 3a). Other properties such as resting membrane potential, action potential threshold, and rheobase were also not significantly different, although they were different in younger animals (Chen et al., 2021) (Supplementary Fig. 3b-d). Therefore, although I228M is predicted to cause DRG hyperexcitability, aged HomNa$_v$1.7^{I228M} mice display a decrease in sodium current, which may be due to the shift in activation/inactivation dynamics of the channel, which prevents development of hyperexcitability.

4.4. RNA sequencing of Nav1.7 I228M mutant DRG neurons shows changes in electrogenesis, pain, and C-LTMR genes

To explore how the Na$_v$1.7^{I228M} mutation affects DRG neurons and try gain insight into the mechanisms of the progressive loss of thermal and pruritogenic sensitivity and development of skin lesions, we performed bulk RNA sequencing of DRG neurons from 20-week-old WT, HetNa$_v$1.7^{I228M}, and HomNa$_v$1.7^{I228M} animals. Many genes were significantly differentially expressed between HomNa$_v$1.7^{I228M} and WT or HetNa$_v$1.7^{I228M} DRG neurons. Multidimensional scaling of the top 500 most variable genes demonstrated that WT and HomNa$_v$1.7^{I228M} samples clustered distinctly, with HetNa$_v$1.7^{I228M} samples residing in between (Fig. 4a). A clustering analysis of the top 100 differentially expressed genes demonstrated that each of the WT, Het, and HomNa$_v$1.7$^{I228M\ DRGs}$ display unique gene expression signatures and cluster accordingly. As the altered behavioral phenotypes are restricted to the HomNa$_v$1.7^{I228M} line, we focus on a comparison of these to WT animals. In addition, we observed that the ratio of significantly up and down-regulated genes was 1:3, indicating that the effect of HomNa$_v$1.7^{I228M} has a strong bias toward down-regulation of gene expression.

A gene ontology analysis for biological processes using the most significantly changed genes, revealed an enrichment of genes associated with ion channel activity, action potentials, and aspects of nervous system development, supporting that transcriptional changes induced by HomNa$_v$1.7^{I228M} evokes many changes beyond those in the channel (Figs. 4a,b; Supplementary Table 2). Indeed, multiple ion channels showed altered expression including sodium, calcium, potassium, and ligand-gated channels. Strikingly similar to Na$_v$1.7 KO mice, *Penk*, the gene encoding proenkephalin which is the precursor for the production of endogenous opioids, was the most up-regulated gene in our dataset, suggesting unexpected commonalities between these two quite distinct (LOF and GOF) mouse models (Minett et al., 2015) (Fig. 4c). Analysis of known Na$_v$1.7 interacting proteins, revealed no altered expression, suggesting that the effects observed are not due to alterations in these factors (Kanellopoulos et al., 2018).

Examination of down-regulated genes revealed a notable change in multiple genes specifically associated with cLTMR sensory neurons (Renthal et al., 2020; Sharma et al., 2020; Reynders et al., 2015). Expression of three canonical cLTMR marker genes: *Th*, *Fam19a4* (*Tafa4*), and *Slc17a8* (*vGlut3*) (Li et al., 2011) were significantly downregulated in HomNa$_v$1.7^{I228M} compared to WT DRG neurons, with

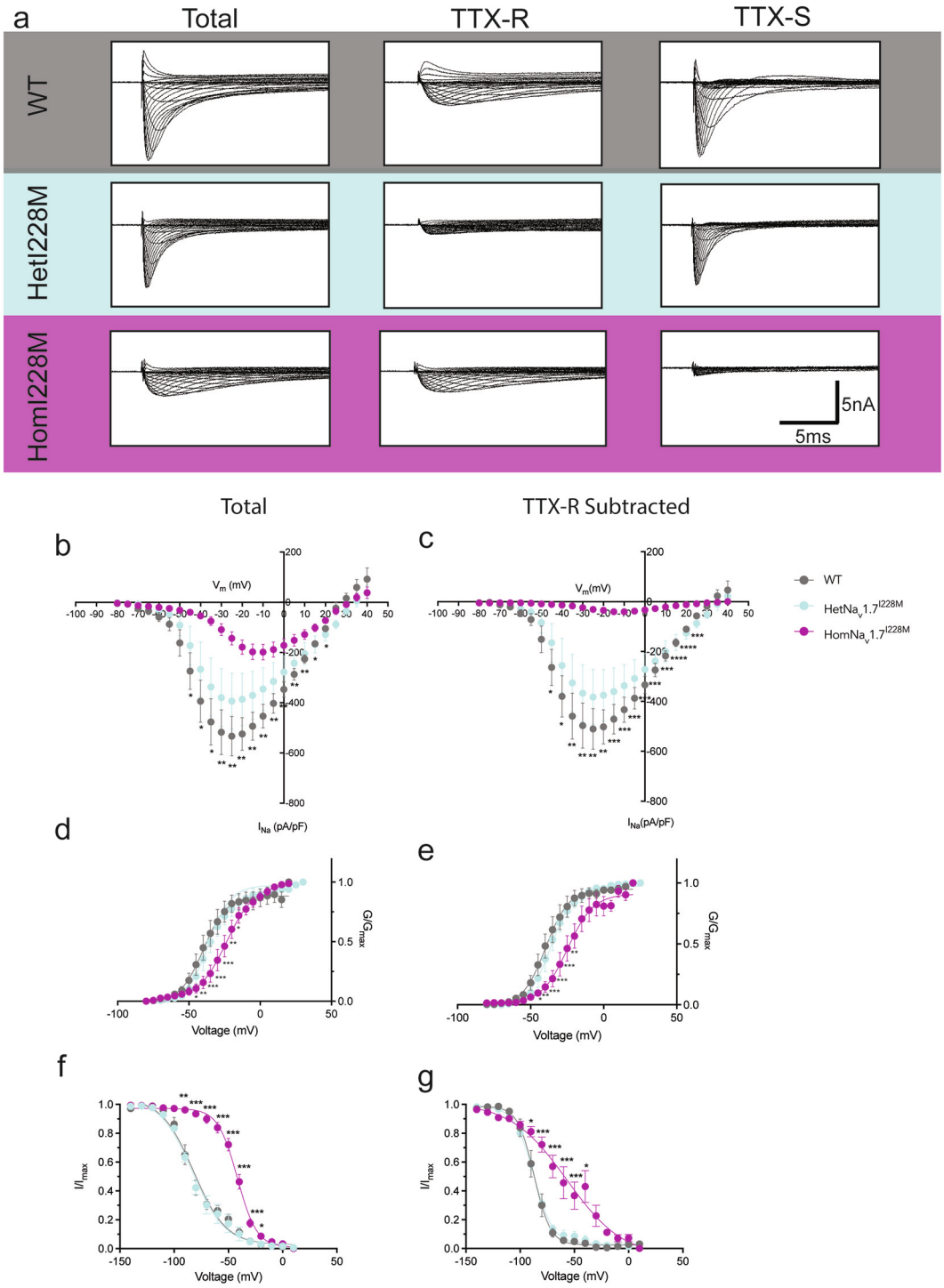

Fig. 3. HomNa$_v$1.7^{I228M} DRG neurons display a paradoxical decrease in Na$^+$ current and a depolarization of the voltage dependence of Na$^+$ channel inactivation. A) Raw traces of Total, TTX-S, and TTX-R current upon different voltages in WT, HetNa$_v$1.7^{I228M} and HomNa$_v$1.7^{I228M} DRG neurons. B—C) Voltage-dependence of the total sodium current (B) and TTX-sensitive (TTX-S) sodium current (C) in WT ($n = 7$, n = 6, respectively), HetNa$_v$1.7^{I228M} ($n = 5$ for both), and HomNa$_v$1.7^{I228M} ($n = 9$; n = 7, respectively) DRG neurons. Both the total and TTX-S sodium current are substantially decreased in HomNa$_v$1.7^{I228M} DRG neurons compared to HetNa$_v$1.7^{I228M} and WT neurons. Two-Way ANOVA with Tukey's posthoc * $p < 0.05$, ** $p < 0.005$, *** $p < 0.0005$, **** $p < 0.00001$. D-E) Voltage-dependence of sodium channel activation (D) and TTX-sensitive sodium channel activation (E in WT (n = 7, n = 6, respectively), HetNa$_v$1.7^{I228M} (n = 5 for both), and HomNa$_v$1.7^{I228M} (n = 9; n = 7, respectively) DRG neurons. No significant differences between genotypes. F-G) Voltage dependence of sodium channel inactivation (F) and TTX-sensitive sodium channel inactivation (G) in WT (n = 7, n = 6, respectively), HetNa$_v$1.7^{I228M} (n = 5 for both), and HomNa$_v$1.7^{I228M} (n = 9; n = 7, respectively) DRG neurons. A significant depolarizing shift in inactivation is observed for total and TTX-S current. For all tests, Two-Way ANOVA with Tukey's posthoc test. B-G) * $p < 0.05$, ** $p < 0.0005$, *** $p < 0.0001$. Statistical details provided in Supplementary Table 1. No changes in RMP, threshold, rheobase, or excitability by current clamp are observed (Supplementary Fig. 3).

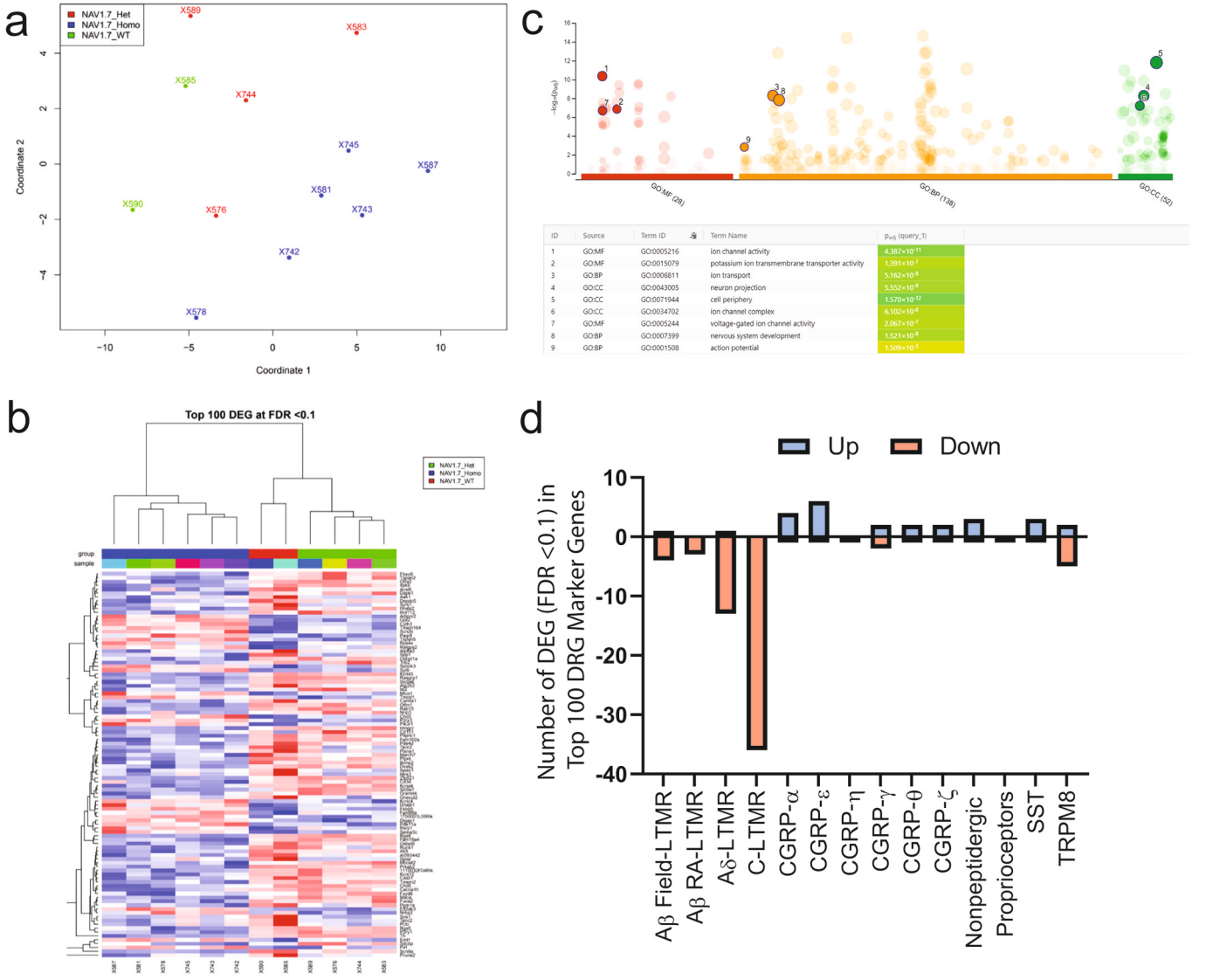

Fig. 4. Transcriptomes of WT, HetNa$_v$1.7^{I228M}, and HomNa$_v$1.7^{I228M} reveal dysregulation of genes controlling electrogenesis and C-LTMR-related gene expression. A) Multidimensional analysis of top 500 genes in transcriptomes of WT, HetNa$_v$1.7^{I228M}, and HomNa$_v$1.7^{I228M} DRGs. Each data point is a sample. B) Cluster dendrogram analysis of top 100 differentially expressed genes (DEGs) demonstrates WT and HetNa$_v$1.7^{I228M} profiles being more closely related than HomNa$_v$1.7^{I228M} which clusters uniquely. C) GO Term Enrichment Analysis of molecular function, biological processes, and cellular compartment (g:Profiler) reveals enrichment of differentially expressed genes that influence electrogenesis within DRG neurons in HomNa$_v$1.7^{I228M}. Selected terms and adjusted *p*-values shown (bottom). Extended data provided in Supplementary Table 2. D) Comparison of top 100 genes enriched in distinct DRG subclasses (Sharma et al., 2020) with the differentially expressed genes in HomNa$_v$1.7^{I228M} DRGs. Upregulated genes have positive, while downregulated, negative values. A large downregulation of C-LTMR gene expression is observed.

Table 1
Electrophysiological Characteristics of WT, HetNa$_v$1.7^{I228M}, and HomNa$_v$1.7^{I228M} DRGs.

	WT	Slope	HetNav1.7 I228M	Slope	WT vs. Het p-value	HomNav1.7 I228M	Slope	WT vs. Hom p-value
Total								
V1/2 Activation (mV)	-40	8.122	−35.8	8.449	*0.2671*	−23.7	9.902	*<0.0001*
V1/2 Inactivation (mV)	−82.1	−14.92	−83.2	−14.98	*0.3625*	−41.7	−8.978	*<0.0001*
TTX								
V1/2 Activation (mV)	−39.8	7.911	−36.2	7.79	*0.907*	−24.8	8.879	*<0.0001*
V1/2 Inactivation (mV)	−87.1	−7.579	−87.5	−8.847	*0.9868*	−56.7	−26.05	*<0.0001*

Th and Slc17a8 being the first and second most significantly changed genes in the dataset. These changes could represent a change in gene expression within cLTMRs, perhaps resulting from a change of their identity, or could be due to a loss of cLTMR neurons.

To determine the effect of HomNa$_v$1.7^{I228M} on DRG subtype specific gene expression, we examined how many of the top 100 enriched genes

from each DRG subtype were altered in HomNa$_v$1.7^{I228M} DRGs. While there was little overlap between the HomNa$_v$1.7^{I228M} induced gene changes and most of the neuronal subtypes, cLTMR gene expression was dysregulated, with 36% of its genes downregulated. To test if this was specific to our mouse model or present in others, we examined genes expressed in C-LTMRs in the transcriptomes of published DRG profiles from Na$_v$1.7cKO mice (Minett et al., 2015). Surprisingly, we found that Na$_v$1.7cKOs also display a significant downregulation of C-LTMR genes, suggesting this is a conserved phenomenon in response to reduced Nav1.7 function (Fig. 5). This finding demonstrates that not only is electrogenesis in DRG neurons altered by the I228M mutation but that alterations occur in a specific DRG subtype over time that may contribute to the complex behavioral phenotype.

4.5. Loss of cLTMR-associated gene expression by RNAScope and qPCR

To confirm these RNASeq results, we performed RNAScope for the cLTMR marker genes *Th* and *Slc17a8*, as well as the pan-neuronal marker *Tubb3,* in fresh-frozen DRG sections from 20-week-old WT and HomNa$_v$1.7^{I228M} animals (Fig. 6a-c, 6j-l). Because of the relatively low numbers of cLTMR neurons present in DRGs at limb levels (C5–7 and L4–5) (Li et al., 2011), we examined thoracic DRGs, and found a striking difference in the proportion of *Th*+/*Tubb3*+ neurons in DRGs from HomNa$_v$1.7^{I228M} mice compared to WT at 20 weeks, in agreement with our RNASeq findings. About 23% of WT thoracic DRG neurons were *Th*+, in accordance with previous reports, compared to only 5.4% of the HomNa$_v$1.7^{I228M} thoracic neurons—representing a 4.5-fold decrease (Fig. 6m, one-way ANOVA followed by Tukey's multiple comparisons test, *p* values as shown in graph).

To determine the timing of the changes in cLTMR gene expression, we repeated the analysis in 2-week-old (P14) and 8-week-old mice of both genotypes (Fig. 6d-i, one-way ANOVA followed by Tukey's multiple comparisons test, p values as shown in graph). Expression of *Th* is not restricted to cLTMRs until P12 (Li et al., 2011); therefore, the youngest mice were assessed at P14 when specificity of the marker is established. Interestingly, we found an age-dependent decrease in the proportion of *Th*+/*Tubb3*+ neurons in HomNa$_v$1.7^{I228M} mice, with 14.1% of the total DRG neurons at P14 and only 7.6% at 8 weeks (Fig. 6m), and as revealed above, only 5.4% at 20 weeks. Even at P14 this represented a 1.65-fold decrease compared to WT, which was significant ($p < 0.0001$). Finally, we also performed qPCR on WT and HomNa$_v$1.7^{I228M} DRGs at 2 and 20 weeks of age and detected a similar reduction in the expression of both *Th* and *Slc17a8* (Fig. 6n, one-way ANOVA followed by Tukey's multiple comparisons test, p values as shown in graph).

5. Discussion

Analysis of aged HomNa$_v$1.7^{I228M} mutant mice reveals somatosensory phenotypes not observed in younger animals, including a decreased/nearly absent sensitivity to noxious thermal and pruritogenic stimuli, and the appearance of skin lesions. This underscores that while these mutations are present from birth in both human patients and mouse models, there are age-dependent effects of their consequences that reveal an undefined aspect of sodium channel biology. Specifically, we did not observe thermal insensitivity and lesions until >18 weeks of age. Likewise, human I228M patients often present with symptoms from 32 to 46 years of age that are variable and in one documented patient, change with age with pain beginning in the trigeminal area and

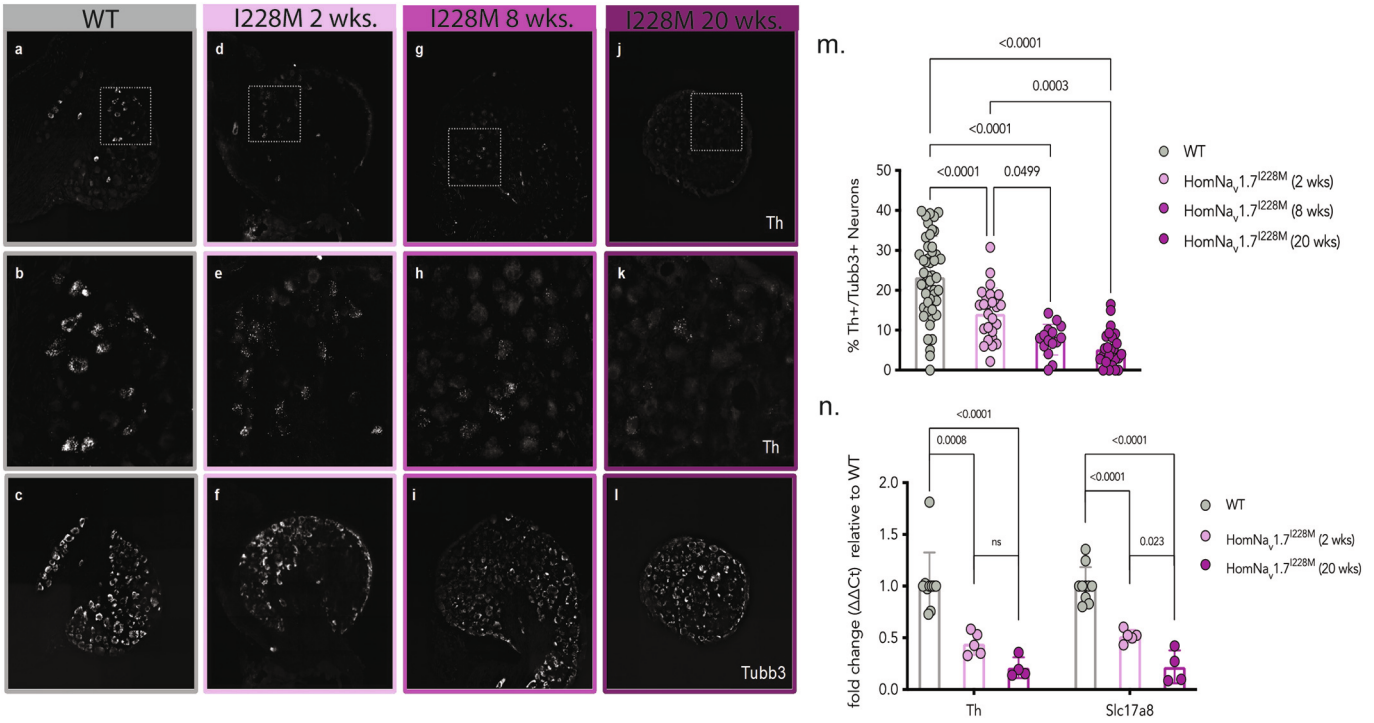

Fig. 5. Decrease in cLTMR-associated gene expression in HomNa$_v$1.7^{I228M} DRGs is progressive. A-L) RNAScope for tyrosine hydroxylase (*Th*), a marker of cLTMRs, and tubulin (*Tubb3*), a pan-neuronal marker. A, D, G, J) Representative images at 10× magnification of a section of a dorsal root ganglion with an RNAScope probe against Th. B, E, H, K) Shows a higher magnification of image of the region outlined above. C, F, I, L) Representative images of RNAScope probe against Tubb3 at 10× magnification of a section of a dorsal root ganglion. A-C) Sections of WT DRGs from 20-week-old mice. D—F) Sections of HomNa$_v$1.7^{I228M} DRGs from 2-week-old mice. G-I) Sections of HomNa$_v$1.7^{I228M} DRGs from 8-week-old mice. J-L) Sections from HomNa$_v$1.7^{I228M} DRGs from 20-week-old mice. M) Quantification of RNAScope data shown in A-L. The percentage of *Th*+/*Tubb3*+ DRG neurons was quantified from 3 mice in each group. Each data point represents percentage. p-values of pairwise comparisons are shown (one-way ANOVA followed by Tukey's multiple comparisons test). N) Reduced expression of *Th* (left) and *Slc17a8* (right) in HomNa$_v$1.7^{I228M} DRG neurons at 2 weeks and 20 weeks by quantitative real-time PCR (qRT-PCR). Each data point represents an individual animal (n = 9 for WT, n = 5 for HomNa$_v$1.7^{I228M} at 2 weeks, *n* = 4 for HomNa$_v$1.7^{I228M} at 20 weeks). p-values for pairwise comparisons are shown (one-way ANOVA followed by Tukey's multiple comparisons test).

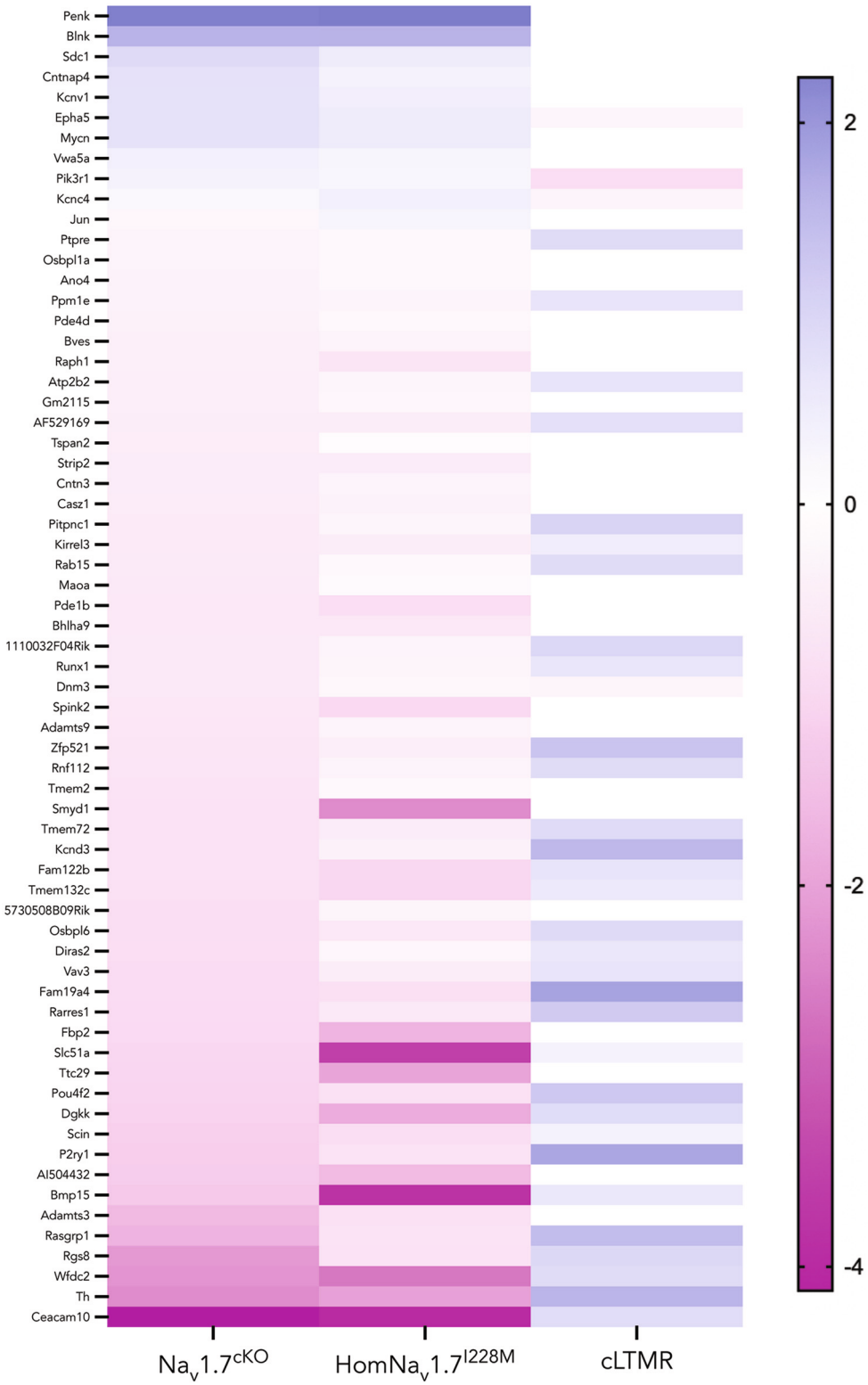

Fig. 6. HomNa$_v$1.7^{I228M} DRGs display a similar decrease in cLTMR-associated gene expression to Na$_v$1.7^{cKO} DRGs. Heat map comparing differentially expressed genes in Na$_v$1.7^{cKO} DRGs (left; from Minett et al. 2015) and HomNa$_v$1.7^{I228M} DRGs (middle) relative to WT. All significantly differentially expressed genes (FDR adjusted p-value <0.05) present in the two datasets are shown, and colored for log$_2$FC values (see color bar). The log$_2$FC values for cLTMRs relative to all other DRG neurons (from (Renthal et al., 2020)) are also shown (right) for all the genes that were differentially expressed in that dataset (FDR adjusted p-value <0.05). Genes not differentially expressed in cLTMRs are shown in white.

extending to the extremities later in life (Estacion et al., 2011). While human patients with the I228M mutation predominately complain of pain-related symptoms, such as a burning pain, this phenotype is complicated by simultaneous reports of numbness and tingling which could be explained either by a LOF in sodium channel function or neuropathy. Our aged mouse model of this GOF mutation clearly reveals a decreased sensitivity to noxious heat stimuli that presents slowly over time. Interestingly, a decreased sensitivity to pain and pruritis as well as tissue lesions, are also observed in heterozygous Na$_v$1.9 L799P (HetNa$_v$1.9^{L799P}) mice and in human patients with the orthologous mutation (L811P). The L799P (human HetNa$_v$1.9^{L811P}) and a second mutation, HetNa$_v$1.9^{L1302F}, from two independent families shift the voltage-dependence of channel activation by ~ −20 mV indicating a GOF phenotype (Huang et al., 2017; Leipold et al., 2013). Paradoxically, these Na$_v$1.9 GOF mutations result in a decreased action potential firing in the DRG neurons, potentially due to a depolarization of the resting

membrane potential that causes inactivation of Nav1.7 and Nav1.8 channels, resulting in an effective cellular LOF (Huang et al., 2017; Ebbinghaus et al., 2020; Leipold et al., 2015). Other putative GOF alleles in patients, such as the HetNa$_v$1.7^{I234T} mutation, also display a complex clinical phenotype, including paroxysmal pain similar to that seen in IEM and PEPD patients but with impaired pain detection, painless scratching and pulling out of teeth, and no reported pain associated with pelvic abscesses, bone fractures, or venipuncture (Meijer et al., 2014; Ahn et al., 2010; Kim et al., 2015; Huang et al., 2018). The HetNa$_v$1.7^{I234T} mutation hyperpolarizes activation by 18 mV and increases average DRG neuronal excitability (Ahn et al., 2010; Yang et al., 2018). However, similar to human HetNa$_v$1.9^{L811P} and HetNa$_v$1.9^{L1302F}, the HetNa$_v$1.7^{I234T} mutation causes hypoexcitability in a subset of DRG neurons because of the large depolarization of their resting membrane potentials. An analogous mechanism could be present in the HomNa$_v$1.7^{I228M} mice. Our Na$_v$1.7, and the Nav1.9 mutant mouse model, show similarities in the timing of the onset of the behavioral phenotype; only mature HetNa$_v$1.9^{L799P} adult mice show a clear phenotype (Ebbinghaus et al., 2020). The activation/inactivation profile of HomNa$_v$1.7^{I228M} DRGs is reminiscent of other IEM/PEPD associated mutations including V948C (Hampl et al., 2016). Future work will determine whether these similarities can extend to an understanding of the changes that occur to HomNa$_v$1.7^{I228M} DRGs. Comparisons of HomNa$_v$1.7^{I228M} mice to the human clinical phenotype may be limited, given that the phenotypes we observe are present only in HomNa$_v$1.7^{I228M} and not HetNa$_v$1.7^{I228M} mice, and there are no known patients homozygous for the Na$_v$1.7^{I228M} mutation. What is clear, is that a GOF mutation in a single Na$_v$ channel is able to produce considerable changes in DRG gene expression and similar transcriptional changes may contribute to the phenotypic variability seen in patients with I228M and other Na$_v$1.7 mutations (Estacion et al., 2011).

Behaviorally, aged HomNa$_v$1.7^{I228M} mice display a remarkably similar phenotype to Na$_v$1.7 LOF or KO mice. This includes an insensitivity to noxious somatosensory stimuli and pruritogens as well as increased *Penk* expression, which increases opioid signaling to produce analgesia (Minett et al., 2015; Isensee et al., 2017). The phenotype we observe is distinct though in that the sensitivity to both innocuous and noxious mechanical stimuli is preserved whereas Nav1.7 LOF mutants display changes in sensitivity to noxious mechanical stimuli (Shields et al., 2018; Chen et al., 2020; Xue et al., 2021). Further, the classic Na$_v$1.7 LOF mutations identified in patients have an early postnatal lethality in mice due to an inability to feed caused by anosmia (Nassar et al., 2004; Weiss et al., 2011). We did not observe similar problems in either the HetNa$_v$1.7^{I228M} or HomNa$_v$1.7^{I228M} mice which may reflect that the LOF in Na$_v$1.7 resulting from the I228M GOF mutation only develops postnatally, and our electrophysiological recordings reveal that the TTX-S sodium conductance in aged mice is reduced but not completely abolished.

A profound decrease in cLTMR-enriched gene expression is present in HomNa$_v$1.7^{I228M} mutant mice including the canonical marker genes *Th*, *Fam19a4*, and *Slc17a8*, along with other cLTMR-enriched genes. cLTMR sensory neurons are primarily associated with pleasant and affective touch (Loken et al., 2009; Vallbo et al., 1999) and only indirectly implicated in pain; for example, a recent study implicated vGlut3 (Slc17a8)-lineage neurons which includes but is not limited to cLTMRs, in the inhibition of touch-evoked itch (Sakai et al., 2020).

Loss of Nav1.7 in C-LTMRs produces a decrease in mechanical sensitivity but minimal changes in thermal sensitivity, with animals preferring cooler temperatures but no change in noxious heat responsiveness (Middleton et al., 2022). However, the somatosensory phenotypes induced by changes in cLTMRs vary, with some models showing increased mechanical sensitivity or no differences (Bohic et al., 2020; Delfini et al., 2013; Francois et al., 2015; Seal et al., 2009). Combinatorial intersectional transgenic approaches to dissect the exact nature of the contributions cLTMRs to behavioral sensitivity should reveal the consequences of a loss of function of these neurons. By analyzing a dataset of differentially expressed genes in sensory-specific Na$_v$1.7 knock-out mice (Nav1.7^{cKO}) by Minett et al., we detected a marked overlap with the differentially expressed genes in HomNa$_v$1.7^{I228M} mutants (Minett et al., 2015). This raises the question why a mutation in Na$_v$1.7 might have a pronounced effect on cLTMRs but not other DRG neuron subtypes. While this remains unclear, single cell sequencing data has shown that Na$_v$1.7 expression is among the highest in cLTMRs compared to other sensory neuron subtypes, while Na$_v$1.8 and Na$_v$1.9 are expressed less in cLTMRs relative to other small diameter DRG neurons (Usoskin et al., 2015). Notably Na$_v$1.8^{KO} and Na$_v$1.9^{KO} DRG neurons show few changes in gene expression and no decrease in *Th* expression or the other cLTMR markers we find here (Minett et al., 2015), suggesting that changes in cLTMR-gene expression are perhaps a unique response only to perturbations in Na$_v$1.7. Our data suggest that in the HomNa$_v$1.7^{I228M} mutants cLTMRs are either progressively lost or change identity as supported by the many unrelated genes enriched in cLTMRs that are co-downregulated together and implies a possible role for this DRG neuron subtype in modulating the function of nociceptors. While a bulk RNA sequencing approach was used to capture a global picture of the changes of a single point mutation on the transcriptional profile, future single-cell sequencing will be needed to resolve how individual subtypes of DRGs change.

Our data suggests that pathogenic SNPs in Na$_v$1.7, in addition to direct effects on channel conductance, may also induce widespread compensatory changes in gene expression, that are likely to contribute to the behavioral phenotype that emerges. Certainly, the heterogenous symptoms and signs observed in patients with IED, PEPD, and SFN, suggest that the mechanism of the diseases and its presentation may reflect changes in the genetic, epigenetic, or environmental landscape. A co-presentation of thermal pain insensitivity, resistance to chloroquine-induced itch and development of skin lesions, as well as the identification of specific effects on cLTMRs, suggests that Na$_v$1.7 mutations have complex effects on multiple different DRG neuronal subtypes including pruriceptors, nociceptors, and low threshold mechanoreceptors. A fixed alteration of Na$_v$1.7 conductance is not, therefore, the only consequence of these mutations, and age-dependent transcriptional and cellular compensatory changes need to be recognized as important contributors to the phenotypes observed in patients and animal models.

Supplementary data to this article can be found online at https://doi.org/10.1016/j.expneurol.2023.114393.

Author contributions

Designed research: NKW, DGT, LC, SDH, SGW, CJW; Performed research: NKW, DGT, SH, JS, MER, RK; Analyzed data: NKW, DGT, JS, SH, RK; Wrote the paper: NKW, DGT, CJW with input from the other authors.

Declaration of Competing Interest

CJW is a founding member of Nocion Therapeutics. The remaining authors declare no conflicts of interest.

Data availability

Requests for raw data can be directed to the corresponding author, Clifford J. Woolf.

Acknowledgements

This work was funded by NIH grant R35NS105076, by the Dr. Miriam and Sheldon G. Adelson Foundation (CJW), an NSF Graduate Research Fellowship Program award (NKW) NS072030, a grant from the Nancy Taylor Foundation (SGW, SDH), and Center Grant B9253—C from the U.S. Department of Veterans Affairs Rehabilitation Research and Development Service (SGW, SDH). The authors thank Aakanksha Jain

for thoughtful discussions regarding this work and Maryam Arab for assistance in mouse breeding. We thank the Harvard Medical School Neurobiology Imaging Facility for consultation and instruments that supported this work. This facility is supported by NINDS P30 Core Center grant NS072030.

References

Ahn, H.S., Dib-Hajj, S.D., Cox, J.J., Tyrrell, L., Elmslie, F.V., Clarke, A.A., et al., 2010. A new Nav1.7 sodium channel mutation I234T in a child with severe pain. Eur. J. Pain 14 (9), 944–950.
Arthur, L., Keen, K., Verriotis, M., Peters, J., Kelly, A., Howard, R.F., et al., 2019. Pediatric Erythromelalgia and SCN9A mutations: systematic review and single-center case series. J. Pediatr. 206 (217–24), e9.
Bohic, M., Marics, I., Santos, C., Malapert, P., Ben-Arie, N., Salio, C., et al., 2020. Loss of bhlha9 impairs thermotaxis and formalin-evoked pain in a sexually dimorphic manner. Cell Rep. 30 (3), 602–10 e6.
Chen, L., Effraim, P.R., Carrara, J., Zhao, P., Dib-Hajj, F.B., Dib-Hajj, S.D., et al., 2020. Pharmacological characterization of a rat Nav1.7 loss-of-function model with insensitivity to pain. Pain. 161 (6), 1350–1360.
Chen, L., Wimalasena, N.K., Shim, J., Han, C., Lee, S.I., Gonzalez-Cano, R., et al., 2021. Two independent mouse lines carrying the Nav1.7 I228M gain-of-function variant display dorsal root ganglion neuron hyperexcitability but a minimal pain phenotype. Pain. 162 (6), 1758–1770.
Cox, J.J., Reimann, F., Nicholas, A.K., Thornton, G., Roberts, E., Springell, K., et al., 2006. An SCN9A channelopathy causes congenital inability to experience pain. Nature. 444 (7121), 894–898.
Delfini, M.C., Mantilleri, A., Gaillard, S., Hao, J., Reynders, A., Malapert, P., et al., 2013. TAFA4, a chemokine-like protein, modulates injury-induced mechanical and chemical pain hypersensitivity in mice. Cell Rep. 5 (2), 378–388.
Dib-Hajj, S.D., Yang, Y., Black, J.A., Waxman, S.G., 2013. The Na(V)1.7 sodium channel: from molecule to man. Nat. Rev. Neurosci. 14 (1), 49–62.
Drenth, J.P., Waxman, S.G., 2007. Mutations in sodium-channel gene SCN9A cause a spectrum of human genetic pain disorders. J. Clin. Invest. 117 (12), 3603–3609.
Ebbinghaus, M., Tuchscherr, L., Segond von Banchet, G., Liebmann, L., Adams, V., Gajda, M., et al., 2020. Gain-of-function mutation in SCN11A causes itch and affects neurogenic inflammation and muscle function in Scn11a+/L799P mice. PLoS One 15 (8), e0237101.
Estacion, M., Han, C., Choi, J.S., Hoeijmakers, J.G., Lauria, G., Drenth, J.P., et al., 2011. Intra- and interfamily phenotypic diversity in pain syndromes associated with a gain-of-function variant of NaV1.7. Mol. Pain 7, 92.
Faber, C.G., Hoeijmakers, J.G., Ahn, H.S., Cheng, X., Han, C., Choi, J.S., et al., 2012. Gain of function Nanu1.7 mutations in idiopathic small fiber neuropathy. Ann. Neurol. 71 (1), 26–39.
Francois, A., Schuetter, N., Laffray, S., Sanguesa, J., Pizzoccaro, A., Dubel, S., et al., 2015. The low-threshold Calcium Channel Cav3.2 determines low-threshold mechanoreceptor function. Cell Rep. 10 (3), 370–382.
Hampl, M., Eberhardt, E., O'Reilly, A.O., Lampert, A., 2016. Sodium channel slow inactivation interferes with open channel block. Sci. Rep. 6, 25974.
Han, C., Dib-Hajj, S.D., Lin, Z., Li, Y., Eastman, E.M., Tyrrell, L., et al., 2009. Early- and late-onset inherited erythromelalgia: genotype-phenotype correlation. Brain. 132 (Pt 7), 1711–1722.
Hoeijmakers, J.G., Merkies, I.S., Gerrits, M.M., Waxman, S.G., Faber, C.G., 2012. Genetic aspects of sodium channelopathy in small fiber neuropathy. Clin. Genet. 82 (4), 351–358.
Hoeijmakers, J.G., Faber, C.G., Merkies, I.S., Waxman, S.G., 2015. Painful peripheral neuropathy and sodium channel mutations. Neurosci. Lett. 596, 51–59.
Huang, J., Han, C., Estacion, M., Vasylyev, D., Hoeijmakers, J.G., Gerrits, M.M., et al., 2014. Gain-of-function mutations in sodium channel Na(v)1.9 in painful neuropathy. Brain. 137 (Pt 6), 1627–1642.
Huang, J., Vanoye, C.G., Cutts, A., Goldberg, Y.P., Dib-Hajj, S.D., Cohen, C.J., et al., 2017. Sodium channel NaV1.9 mutations associated with insensitivity to pain dampen neuronal excitability. J. Clin. Invest. 127 (7), 2805–2814.
Huang, J., Mis, M.A., Tanaka, B., Adi, T., Estacion, M., Liu, S., et al., 2018. Atypical changes in DRG neuron excitability and complex pain phenotype associated with a Nav1.7 mutation that massively hyperpolarizes activation. Sci. Rep. 8 (1), 1811.
Isensee, J., Krahe, L., Moeller, K., Pereira, V., Sexton, J.E., Sun, X., et al., 2017. Synergistic regulation of serotonin and opioid signaling contributes to pain insensitivity in Nav1.7 knockout mice. Sci. Signal. 10 (461).
Kanellopoulos, A.H., Koenig, J., Huang, H., Pyrski, M., Millet, Q., Lolignier, S., et al., 2018. Mapping protein interactions of sodium channel Na(V)1.7 using epitope-tagged gene-targeted mice. EMBO J. 37 (3), 427–445.
Kim, D.T., Rossignol, E., Najem, K., Ospina, L.H., 2015. Bilateral congenital corneal anesthesia in a patient with SCN9A mutation, confirmed primary erythromelalgia, and paroxysmal extreme pain disorder. J. AAPOS. 19 (5), 478–479.
Klein, J.P., Tendi, E.A., Dib-Hajj, S.D., Fields, R.D., Waxman, S.G., 2003. Patterned electrical activity modulates sodium channel expression in sensory neurons. J. Neurosci. Res. 74 (2), 192–198.
Kuhn, H., Kappes, L., Wolf, K., Gebhardt, L., Neurath, M.F., Reeh, P., et al., 2020. Complementary roles of murine NaV1.7, NaV1.8 and NaV1.9 in acute itch signalling. Sci. Rep. 10 (1), 2326.
Lee, S.I., Hoeijmakers, J.G.J., Faber, C.G., Merkies, I.S.J., Lauria, G., Waxman, S.G., 2020. The small fiber neuropathy NaV1.7 I228M mutation: impaired neurite integrity via bioenergetic and mitotoxic mechanisms, and protection by dexpramipexole. J. Neurophysiol. 123 (2), 645–657.
Leipold, E., Liebmann, L., Korenke, G.C., Heinrich, T., Giesselmann, S., Baets, J., et al., 2013. A de novo gain-of-function mutation in SCN11A causes loss of pain perception. Nat. Genet. 45 (11), 1399–1404.
Leipold, E., Hanson-Kahn, A., Frick, M., Gong, P., Bernstein, J.A., Voigt, M., et al., 2015. Cold-aggravated pain in humans caused by a hyperactive NaV1.9 channel mutant. Nat. Commun. 6, 10049.
Li, L., Rutlin, M., Abraira, V.E., Cassidy, C., Kus, L., Gong, S., et al., 2011. The functional organization of cutaneous low-threshold mechanosensory neurons. Cell. 147 (7), 1615–1627.
Loken, L.S., Wessberg, J., Morrison, I., McGlone, F., Olausson, H., 2009. Coding of pleasant touch by unmyelinated afferents in humans. Nat. Neurosci. 12 (5), 547–548.
Marchi, M., Provitera, V., Nolano, M., Romano, M., Maccora, S., D'Amato, I., et al., 2018. A novel SCN9A splicing mutation in a compound heterozygous girl with congenital insensitivity to pain, hyposmia and hypogeusia. J. Peripher. Nerv. Syst. 23 (3), 202–206.
Meijer, I.A., Vanasse, M., Nizard, S., Robitaille, Y., Rossignol, E., 2014. An atypical case of SCN9A mutation presenting with global motor delay and a severe pain disorder. Muscle Nerve 49 (1), 134–138.
Middleton, S.J., Perini, I., Themistocleous, A.C., Weir, G.A., McCann, K., Barry, A.M., et al., 2022. Nav1.7 is required for normal C-low threshold mechanoreceptor function in humans and mice. Brain. 145 (10), 3637–3653.
Minett, M.S., Pereira, V., Sikandar, S., Matsuyama, A., Lolignier, S., Kanellopoulos, A.H., et al., 2015. Endogenous opioids contribute to insensitivity to pain in humans and mice lacking sodium channel Nav1.7. Nat. Commun. 6, 8967.
Nassar, M.A., Stirling, L.C., Forlani, G., Baker, M.D., Matthews, E.A., Dickenson, A.H., et al., 2004. Nociceptor-specific gene deletion reveals a major role for Nav1.7 (PN1) in acute and inflammatory pain. Proc. Natl. Acad. Sci. U. S. A. 101 (34), 12706–12711.
Persson, A.K., Liu, S., Faber, C.G., Merkies, I.S., Black, J.A., Waxman, S.G., 2013. Neuropathy-associated Nav1.7 variant I228M impairs integrity of dorsal root ganglion neuron axons. Ann. Neurol. 73 (1), 140–145.
Raudvere, U., Kolberg, L., Kuzmin, I., Arak, T., Adler, P., Peterson, H., et al., 2019. G: profiler: a web server for functional enrichment analysis and conversions of gene lists (2019 update). Nucleic Acids Res. 47 (W1). W191-W8.
Renthal, W., Tochitsky, I., Yang, L., Cheng, Y.C., Li, E., Kawaguchi, R., et al., 2020. Transcriptional reprogramming of distinct peripheral sensory neuron subtypes after axonal injury. Neuron. 108 (1), 128–44 e9.
Reynders, A., Mantilleri, A., Malapert, P., Rialle, S., Nidelet, S., Laffray, S., et al., 2015. Transcriptional profiling of cutaneous MRGPRD free nerve endings and C-LTMRs. Cell Rep. 10 (6), 1007–1019.
Ritchie, M.E., Phipson, B., Wu, D., Hu, Y., Law, C.W., Shi, W., et al., 2015. Limma powers differential expression analyses for RNA-sequencing and microarray studies. Nucleic Acids Res. 43 (7), e47.
Rush, A.M., Cummins, T.R., Waxman, S.G., 2007. Multiple sodium channels and their roles in electrogenesis within dorsal root ganglion neurons. J. Physiol. 579 (Pt 1), 1–14.
Sakai, K., Sanders, K.M., Lin, S.H., Pavlenko, D., Funahashi, H., Lozada, T., et al., 2020. Low-threshold mechanosensitive VGLUT3-lineage sensory neurons mediate spinal inhibition of itch by touch. J. Neurosci. 40 (40), 7688–7701.
Seal, R.P., Wang, X., Guan, Y., Raja, S.N., Woodbury, C.J., Basbaum, A.I., et al., 2009. Injury-induced mechanical hypersensitivity requires C-low threshold mechanoreceptors. Nature. 462 (7273), 651–655.
Sharma, N., Flaherty, K., Lezgiyeva, K., Wagner, D.E., Klein, A.M., Ginty, D.D., 2020. The emergence of transcriptional identity in somatosensory neurons. Nature. 577 (7790), 392–398.
Shields, S.D., Deng, L., Reese, R.M., Dourado, M., Tao, J., Foreman, O., et al., 2018. Insensitivity to pain upon adult-onset deletion of Nav1.7 or its blockade with selective inhibitors. J. Neurosci. 38 (47), 10180–10201.
Sun, J., Li, L., Yang, L., Duan, G., Ma, T., Li, N., et al., 2020. Novel SCN9A missense mutations contribute to congenital insensitivity to pain: unexpected correlation between electrophysiological characterization and clinical phenotype. Mol. Pain 16, 1744806920923881.
Usoskin, D., Furlan, A., Islam, S., Abdo, H., Lonnerberg, P., Lou, D., et al., 2015. Unbiased classification of sensory neuron types by large-scale single-cell RNA sequencing. Nat. Neurosci. 18 (1), 145–153.
Vallbo, A.B., Olausson, H., Wessberg, J., 1999. Unmyelinated afferents constitute a second system coding tactile stimuli of the human hairy skin. J. Neurophysiol. 81 (6), 2753–2763.
Weiss, J., Pyrski, M., Jacobi, E., Bufe, B., Willnecker, V., Schick, B., et al., 2011. Loss-of-function mutations in sodium channel Nav1.7 cause anosmia. Nature. 472 (7342), 186–190.
Wimalasena, N.K., Milner, G., Silva, R., Vuong, C., Zhang, Z., Bautista, D.M., et al., 2021. Dissecting the precise nature of itch-evoked scratching. Neuron. 109 (19), 3075–87 e2.
Xue, Y., Chidiac, C., Herault, Y., Gaveriaux-Ruff, C., 2021. Pain behavior in SCN9A (Nav1.7) and SCN10A (Nav1.8) mutant rodent models. Neurosci. Lett. 753, 135844.
Yang, Y., Huang, J., Mis, M.A., Estacion, M., Macala, L., Shah, P., et al., 2016. Nav1.7-A1632G Mutation from a Family with Inherited Erythromelalgia: Enhanced Firing of Dorsal Root Ganglia Neurons Evoked by Thermal Stimuli. J. Neurosci. 36 (28), 7511–7522.
Yang, Y., Adi, T., Effraim, P.R., Chen, L., Dib-Hajj, S.D., Waxman, S.G., 2018. Reverse pharmacogenomics: carbamazepine normalizes activation and attenuates thermal

hyperexcitability of sensory neurons due to Nav 1.7 mutation I234T. Br. J. Pharmacol. 175 (12), 2261–2271.